Mon. Not. R. Astron. Soc. **368,** 809–818 (2006) doi:10.1111/j.1365-2966.2006.10168.x

Asteroid orbits using phase-space volumes of variation

K. Muinonen,⋆ J. Virtanen, M. Granvik and T. Laakso
Observatory, PO Box 14, FI-00014 University of Helsinki, Finland

Accepted 2006 February 2. Received 2006 February 2; in original form 2004 December 22

ABSTRACT

We present a statistical orbit computation technique for asteroids with transitional observational data, that is, a moderate number of data points spanning a moderate observational time interval. With the help of local least-squares solutions in the phase space of the orbital elements, we map the volume of variation as a function of one or more of the elements. We sample the resulting volume using a Monte Carlo technique and, with proper weights for the sample orbital elements, characterize the six-dimensional orbital-element probability density function. The volume-of-variation (VOV) technique complements the statistical ranging technique for asteroids with exiguous observational data (short time intervals and/or small numbers of observations) and the least-squares technique for extensive observational data. We show that, asymptotically, results using the new technique agree closely with those from ranging and least squares. We apply the technique to the near-Earth object 2004 HA_{39}, the main-belt object 2004 QR and the transneptunian object 2002 CX_{224} recently observed at the Nordic Optical Telescope on La Palma, illustrating the potential of the technique in ephemeris prediction. The VOV technique helps us assess the phase transition in orbital-element probability densities, that is, the non-linear collapse of wide orbital-element distributions to narrow localized ones. For the three objects above, the transition takes place for observational time intervals of the order of 10 h, 5 d and 10 months, respectively, emphasizing the significance of the orbital-arc fraction covered by the observations.

Key words: methods: numerical – methods: statistical – celestial mechanics – minor planets, asteroids.

1 INTRODUCTION

Numerous novel asteroid orbit computation techniques have been developed in recent years. They have been inspired by, for example, the collision risk from near-Earth objects (NEOs) and the recognition that the ordinary least-squares approach fails to describe the orbital uncertainties arising in the inverse problem of asteroid orbit computation. For transneptunian objects (TNOs), orbit determination has been challenging because of the particularly long orbital periods involved whereas, for main-belt objects (MBOs), difficulties have accumulated because of the large numbers of objects observed over single apparitions, only creating an increasing identification problem.

Although the asteroid orbit determination problem dates back to Gauss (1809, see also Danby 1992) and further, the statistical inverse problem of deriving asteroid orbits from astrometric observations was only recently established by Muinonen & Bowell (1993). Although most of their work concentrated on asteroids with extensive observational data, they brought up the non-Gaussian characteristics of the orbital-element probability density functions (PDFs). They offered a Monte Carlo (MC) technique for assessing non-Gaussian orbital-element PDFs. The Gaussian PDFs followed from what they called the linear approximation consisting of the orbital elements from non-linear least squares and the accompanying covariance matrix based on linearization (LSL, non-linear least squares with linearization). The MC technique drew trial orbital elements using LSL extended over larger phase-space volumes using a scaling coefficient to be iterated for the full coverage of the orbit solution space. The application of the technique was constrained to mildly non-Gaussian orbital-element PDFs – the deviations from Gaussian PDFs were illustrated using covariance matrices resulting from MC orbital-element moment computation.

Before the work on the statistical inverse problem above, miscellaneous practical line-of-variation (LOV) techniques were already in use in several orbit computation centres. These techniques derived from the notion that, in asteroid ephemeris predictions, deviations between the computed sky-plane predictions and the actual observations took typically place along the projection of the orbit of an asteroid on the sky-plane, suggesting that the predominating uncertainties were those in the semimajor axis (and thus the mean motion) as well as in the mean anomaly.

⋆E-mail: Karri.Muinonen@Helsinki.Fi

Bowell et al. (1993) developed the LOV technique in the perihelion distance, initiating searches for the then-lost asteroid (719) Albert. The perihelion distance was varied systematically and the remaining orbital elements were fitted, in least-squares sense, for the given values of the perihelion distance. Negative observations, that is, observations of relevant sky-plane regions with Albert not detected were utilized to reduce the perihelion distance domain available for Albert. Unfortunately, systematic archival searches for Albert failed at the time – Albert was later recovered serendipitously as $2000\,\mathrm{JW}_8$ by the Spacewatch Project of the University of Arizona.

Muinonen (1996) returned to LSL describing the LOV technique for Gaussian PDFs. In that case, the solution of the orbital covariance eigenproblem for (719) Albert and comet Hale–Bopp (Bailey et al. 1996) showed that, with the astrometric observations available at that time, there was a single predominating eigenvalue with the corresponding eigenvector for both objects. In continuation, Muinonen, Milani & Bowell (1997) concentrated on a larger number of single-apparition asteroids and concluded that the linear approximation faced difficulties in the case of exiguous observational data, that is, short observational time intervals and/or small numbers of observations.

There were two main solutions to tackle the non-linearities. On one hand, Virtanen, Muinonen & Bowell (2001) came up with the so-called statistical-ranging technique (Ranging) that resulted in a rigorous MC solution to the inverse problem concerning exiguous observational data. On the other hand, Milani (1999) refined the LOV techniques substantially and developed a technique that, rather than stepping forwards in a certain mapping orbital element, moved along the line of variation in the search of multiple solutions. Milani's LOV technique became routinely applicable to large numbers of asteroids, in particular, in ephemeris prediction and impact probability computation (Milani 1999; Milani et al. 2002). More recently, Milani et al. (2004, 2005) have taken a geometric approach to uncertainty estimation. For what they term 'very short arcs', they use a set of virtual asteroids to describe the uncertainty region by triangulation of the range and radial velocity (or range-rate) plane.

Whereas Ranging assesses the entire six-dimensional phase-space volume of orbit solutions and thus constitutes a full solution to the inverse problem, the LOV techniques have remained one dimensional. In the present paper, we develop a six-dimensional volume-of-variation (VOV) technique that characterizes the full orbit-solution space using one or more mapping orbital elements and subsequent MC sampling. It generalizes the former techniques to account for the remaining dimensions of the inverse problem. Furthermore, VOV improves on the speed of Ranging for increasing observational time intervals. VOV is closely related to LOV and other LOV techniques: it is based on a sequence of local linear approximations along a line or plane of variation.

Closely resembling the initialization part of VOV, Chesley (2005) introduces a plane-of-variation technique that utilizes the range and range rate as the orbital elements to be systematically varied. In that technique, a two-dimensional plane of orbital elements is obtained using local linear approximations for the remaining four parameters. Each range and range-rate solution is weighted by an exponential factor containing the χ^2 of the fit. However, the four remaining dimensions of the inverse problem are not treated.

Our preliminary studies have pointed out that the evolution of orbital uncertainties as a function of increasing observational time interval (or rather, the covered orbital arc) is highly non-linear across a rather narrow transition regime. Because the occurrence of this collapse in the extent of the orbital distribution seems to be quite abrupt, as it first was discovered for improving observational accuracy (Muinonen & Virtanen 2002) and later recognized also for increasing observational data (Virtanen et al. 2005), we have termed the phenomenon phase transition. The existence of such a transition effect suggests that different computational methods could be used to assess the uncertainties before, at and after the transition.

The phase transition can be characterized as being a transition from disorder to order with increasing time interval (cf. Reichl 1980). There are various possible choices for the so-called order parameter characterizing the transition. One choice is the extent (or hypervolume) of the phase space covered by orbit solutions. Another can be constructed by discretizing the phase space into finite cells (or states) and computing the probability mass (or normalized occupation number) for each cell. At the phase transition point, there is a rapid condensation of probability mass into a small subset of cells. Finally, as there is a continuum of possible states, the PDF itself can serve as the order parameter.

We compare VOV sampling on one hand to the least-squares covariance analysis, which is known to fail to describe the uncertainties for very short time intervals, and on the other hand to the non-linear Ranging which has turned out to be a computationally impractical way to sample the uncertainties for longer intervals. In what follows for the NEO $2004\,\mathrm{HA}_{39}$, MBO $2004\,\mathrm{QR}$ and TNO $2002\,\mathrm{CX}_{224}$, we illustrate VOV sampling by using Keplerian orbital elements and the semimajor axis as the sole mapping element.

In Section 2, we outline the inverse problem of deriving orbital element PDFs for asteroid orbits from astrometric observations. We describe the global and local linear approximations and develop a VOV sampling technique initialized using the local linear approximations. Section 3 illustrates the application of VOV to small Solar system bodies with transitional observational data. Conclusions and future prospects are assessed in Section 4.

2 INVERSE PROBLEM

2.1 Orbital-element probability density

We denote the osculating orbital elements of an asteroid at a given epoch t_0 by the 6-vector $\boldsymbol{P}$. For Keplerian elements, $\boldsymbol{P} = (a, e, i, \Omega, \omega, M_0)^{\mathrm{T}}$ (T is transpose) and the elements are, respectively, the semimajor axis, eccentricity, inclination, longitude of ascending node, argument of perihelion and mean anomaly. The three angular elements i, Ω and ω are currently referred to the ecliptic at equinox J2000.0. For Cartesian elements, $\boldsymbol{P} = (X, Y, Z, \dot{X}, \dot{Y}, \dot{Z})^{\mathrm{T}}$ where, in a given Cartesian reference frame, the coordinates $(X, Y, Z)^{\mathrm{T}}$ denote the position and the coordinates $(\dot{X}, \dot{Y}, \dot{Z})^{\mathrm{T}}$ the velocity.

The orbital-element PDF p_{p} is proportional to the a priori (p_{pr}) and observational error (p_ϵ) PDFs, the latter being evaluated for the sky-plane ('Observed − Computed') residuals $\Delta\psi(\boldsymbol{P})$ (Muinonen & Bowell 1993),

$$p_{\mathrm{p}}(\boldsymbol{P}) \propto p_{\mathrm{pr}}(\boldsymbol{P}) p_\epsilon(\Delta\psi(\boldsymbol{P})), \tag{1}$$

where p_ϵ can usually be assumed to be Gaussian. For the mathematical form of p_{p} to be invariant in transformations from one orbital element set to another (e.g. from Keplerian to equinoctial or Cartesian), we regularize the statistical analysis by Jeffreys' a priori PDF (Jeffreys 1946; see also Muinonen, Virtanen & Bowell 2001),

$$\begin{aligned} p_{\mathrm{pr}}(\boldsymbol{P}) &\propto \sqrt{\det \boldsymbol{\Sigma}^{-1}(\boldsymbol{P})}, \\ \boldsymbol{\Sigma}^{-1}(\boldsymbol{P}) &= \boldsymbol{\Phi}(\boldsymbol{P})^{\mathrm{T}} \boldsymbol{\Lambda}^{-1} \boldsymbol{\Phi}(\boldsymbol{P}), \end{aligned} \tag{2}$$

where $\mathbf{\Sigma}^{-1}$ is the information matrix (or the inverse covariance matrix) evaluated for the orbital elements $\boldsymbol{P}$, $\mathbf{\Phi}$ contains the partial derivatives of right ascension (RA) and declination (Dec.) with respect to the orbital elements, and $\mathbf{\Lambda}$ is the covariance matrix for the observational errors. By the choice of the a priori PDF, the transformation of rigorous PDFs becomes analogous to that of Gaussian PDFs.

The final a posteriori orbital-element PDF is, with the help of the χ^2 evaluated for the elements $\boldsymbol{P}$,

$$p_{\rm p}(\boldsymbol{P}) \propto \sqrt{\det \mathbf{\Sigma}^{-1}(\boldsymbol{P})}\ \exp\left[-\frac{1}{2}\chi^2(\boldsymbol{P})\right],$$
$$\chi^2(\boldsymbol{P}) = \Delta\psi^{\rm T}(\boldsymbol{P})\mathbf{\Lambda}^{-1}\Delta\psi(\boldsymbol{P}). \quad (3)$$

As a consequence of securing the invariance in orbital-element transformations, e.g. ephemeris uncertainties and collision probabilities based on the orbital-element PDF are independent of the choice of the orbital-element set (Virtanen & Muinonen 2006). Note that assuming constant $p_{\rm pr}$ is acceptable, when the exponent part of equation (3) confines the PDF into a phase-space regime, where the determinant part reduces to a constant.

2.2 Linear approximations

In the validity regime of LSL, that is, the non-linear least squares with linearized covariances (or the global linear approximation),

$$\chi^2(\boldsymbol{P}) \approx \chi^2(\boldsymbol{P}_{\rm ls}) + \Delta\boldsymbol{P}^{\rm T}\mathbf{\Sigma}^{-1}(\boldsymbol{P}_{\rm ls})\Delta\boldsymbol{P},$$
$$\Delta\boldsymbol{P} = \boldsymbol{P} - \boldsymbol{P}_{\rm ls},$$
$$\det\mathbf{\Sigma}^{-1}(\boldsymbol{P}) \approx \det\mathbf{\Sigma}^{-1}(\boldsymbol{P}_{\rm ls}), \quad (4)$$

where $\boldsymbol{P}_{\rm ls}$ denotes the least-squares orbital elements. The resulting orbital-element PDF is Gaussian,

$$p_{\rm p}(\boldsymbol{P}) \propto \sqrt{\det\mathbf{\Sigma}^{-1}(\boldsymbol{P}_{\rm ls})} \times \exp\left[-\frac{1}{2}\Delta\boldsymbol{P}^{\rm T}\mathbf{\Sigma}^{-1}(\boldsymbol{P}_{\rm ls})\Delta\boldsymbol{P}\right]. \quad (5)$$

The least-squares orbital elements $\boldsymbol{P}_{\rm ls}$ and their covariance matrix $\mathbf{\Sigma}$ constitute the full, concise solution to the inverse problem.

A mathematically strict LSL would involve the simultaneous linearization of the exponential and determinant parts of the rigorous a posteriori PDF. Although computationally accessible, first, the strict linearization would result in the abandonment of the commonly used differential correction procedure to obtain the best-fitting orbit and, secondly, it would inevitably introduce second-order partial derivatives into the search for the orbital elements at the tip of the a posteriori PDF. Sacrificing some of the mathematical beauty, we adopt the more practical definition for LSL in equation (4).

The a posteriori PDF in equation (3) allows the derivation of a local linear approximation in the orbital-element phase space. We can select one or more of the elements as 'the elements to be varied' systematically and derive a linear approximation for 'the remaining elements to be fitted'. For simplicity, we illustrate the local linear approximations below in the case of a single mapping element and note that the formulation is analogous for more numerous mapping elements.

We rewrite the a posteriori PDF in equation (3) explicitly in terms of the mapping element $P_{\rm m}$ and the five remaining elements $\boldsymbol{P}'$ (here and below, the prime denotes five-dimensional quantities),

$$p_{\rm p}(P_{\rm m}, \boldsymbol{P}') \propto \sqrt{\det\mathbf{\Sigma}^{-1}(P_{\rm m}, \boldsymbol{P}')} \times \exp\left[-\frac{1}{2}\chi^2(P_{\rm m}, \boldsymbol{P}')\right],$$
$$\chi^2(P_{\rm m}, \boldsymbol{P}') = \Delta\psi^{\rm T}(P_{\rm m}, \boldsymbol{P}')\mathbf{\Lambda}^{-1}\Delta\psi(P_{\rm m}, \boldsymbol{P}'). \quad (6)$$

For a given $P_{\rm m}$, we define the local linear approximation as follows.

$$p_{\rm p}(P_{\rm m}, \boldsymbol{P}') \propto \sqrt{\det\mathbf{\Sigma}^{-1}(P_{\rm m}, \boldsymbol{P}'_{\rm ls})}\exp\left[-\frac{1}{2}\chi^2(P_{\rm m}, \boldsymbol{P}'_{\rm ls})\right] \times \exp\left[-\frac{1}{2}\Delta\boldsymbol{P}'^{\rm T}\mathbf{\Sigma}'^{-1}(P_{\rm m}, \boldsymbol{P}'_{\rm ls})\Delta\boldsymbol{P}'\right],$$
$$\Delta\boldsymbol{P}' = \boldsymbol{P}' - \boldsymbol{P}'_{\rm ls}(P_{\rm m}), \quad (7)$$

where $\boldsymbol{P}'_{\rm ls} = \boldsymbol{P}'_{\rm ls}(P_{\rm m})$ is the local least-squares solution for the elements $\boldsymbol{P}'$. Note that both $\mathbf{\Sigma}^{-1}$ and $\mathbf{\Sigma}'^{-1}$ enter the local linear approximations above. The sequence of orbital elements $P_{\rm m}$, $\boldsymbol{P}'_{\rm ls}(P_{\rm m})$ defines the line of variation in the orbital-element phase space.

The local 5×5 covariance matrix $\mathbf{\Sigma}'$ is recomputed at the local least-squares solution and defines a hyperellipsoid centred at these elements (cf. Muinonen 1996),

$$\Delta\chi^2(\boldsymbol{P}') = \Delta\boldsymbol{P}'^{\rm T}\mathbf{\Sigma}'^{-1}\Delta\boldsymbol{P}' = \Delta\chi_0^2, \quad (8)$$

where $\Delta\chi_0^2$ is a constant. The boundaries of, for example, the 68.3 or 95.4 per cent probability hyperellipsoids are $\Delta\chi_0^2 \approx 5.89$ or $\Delta\chi_0^2 \approx 11.3$, respectively.

It is convenient to express the differences $\Delta\boldsymbol{P}'$ in terms of the values of s.d. $\sigma'_j = \sqrt{\Sigma'_{jj}}(j = 1, \ldots, 5)$ and to utilize the dimensionless correlation matrix $\mathbf{C}'$; with the help of the diagonal s.d. matrix $\mathbf{S}'$,

$$\Delta\boldsymbol{Q}' = \mathbf{S}'^{-1}\Delta\boldsymbol{P}',$$
$$\mathbf{C}' = \mathbf{S}'^{-1}\mathbf{\Sigma}'\mathbf{S}'^{-1},$$
$$S'_{jk} = \sigma'_j\,\delta_{jk}, \quad j, k = 1, \ldots, 6, \quad (9)$$

where δ_{jk} is the Kronecker symbol. The hyperellipsoid is thus defined by

$$\Delta\boldsymbol{Q}'^{\rm T}\mathbf{C}'^{-1}\Delta\boldsymbol{Q}' = \Delta\chi_0^2, \quad (10)$$

where all the parameters are dimensionless. The eigenvalues λ'_j $(j = 1, \ldots, 5)$ for the correlation matrix $\mathbf{C}'$ are normalized variances along the principal axes of the hyperellipsoid, the directions of the axes being given by the orthonormal eigenvectors $\boldsymbol{X}'_j$,

$$\mathbf{C}'\boldsymbol{X}'_j = \lambda'_j\boldsymbol{X}'_j, \quad j = 1, \ldots, 5. \quad (11)$$

Since $\mathbf{C}'$ is a real and symmetric matrix, the eigenproblem can be solved via Jacobi transformations (Press et al. 1994).

Once the eigenvalues and eigenvectors are available, the shape and orientation of the hyperellipsoid become transparent. For example, points on the hypersurface in the directions of the principal axes corresponding to a given $\Delta\chi_0^2$ are

$$\boldsymbol{P}'^{\pm}_j = \boldsymbol{P}'_{\rm ls} \pm \sqrt{\Delta\chi_0^2\lambda'_j}\mathbf{S}'\boldsymbol{X}'_j, \quad j = 1, \ldots, 5. \quad (12)$$

The local linear approximations allow the study of the validity of the global linear approximation: if the local least-squares solutions do not fall on a straight line or if the local covariances differ, the global linear approximation must be rejected.

On one hand, the straightforward application of the local linear approximations suffers from shortcomings: it requires the storage of large numbers (several hundreds to thousands) of mapping elements, covariance matrices and weight factors, without certainty

of validity across the regime studied for the mapping element. On the other hand, as shown below, the local linear approximations can constitute an invaluable guide, in the orbital-element phase space, to the proximity of orbit solutions for the rigorous inverse problem.

The validity of the local linear approximations depends on the set of orbital elements selected. Whereas Keplerian elements are attractive because of their conceptual clarity, Cartesian elements can in general be preferable. We can offer the following reasoning based on Gaussian random variables to support a choice of a certain Cartesian set of orbital elements. Select an epoch for the orbital elements coinciding with one of the observation dates close to the mid-point of the observational time interval. Consider then orbital elements that are the Cartesian position vector $(X, Y, Z)^{\mathrm{T}}$ and velocity vector $(\dot{X}, \dot{Y}, \dot{Z})^{\mathrm{T}}$, where the z-axis points in the topocentric direction of the object and the x- and y-axes coincide with the RA and Dec. axes, respectively. In particular for exiguous observational data, the potential Gaussian characteristics of the four transverse orbital elements $(X, Y)^{\mathrm{T}}$ and $(\dot{X}, \dot{Y})^{\mathrm{T}}$ are suggested by the sum rule for Gaussian random variables: adding or subtracting Gaussian random variables results in random variables that are Gaussian. Here, $(X, Y)^{\mathrm{T}}$ and $(\dot{X}, \dot{Y})^{\mathrm{T}}$ can be taken as estimates of the mean position and position differences on the sky plane. Thus, the two natural mapping elements are the line-of-sight distance (range) and velocity (radial velocity or range rate) of the object at the given epoch (cf. Chesley 2005).

2.3 Sampling the volumes of variation

It is our goal to draw sample orbits from the rigorous orbital-element PDF with the help of the local linear approximations. First, we specify the variation interval for the mapping element with the help of the covariance matrix $\boldsymbol{\Sigma}$ derived in LSL and emphasize that the variation interval must be subject to iteration.

$$P_{\mathrm{m}} \in [P_{\mathrm{m,ls}} - \Delta P_{\mathrm{m}}, P_{\mathrm{m,ls}} + \Delta P_{\mathrm{m}}], \tag{13}$$

where $P_{\mathrm{m,ls}}$ is the global least-squares value for the mapping element and ΔP_{m} is the half-width of the variation interval. For example, as a starting point for ΔP_{m}, one may utilize the one-dimensional 3σ (or 99.7 per cent) variation interval as given by LSL. Secondly, the remaining elements are sampled with the help of the local intervals of variation so that

$$\boldsymbol{P}' = \boldsymbol{P}'_{\mathrm{ls}}(P_{\mathrm{m}}) + \sum_{j=1}^{5} (1 - 2r_j)\sqrt{\Delta\tilde{\chi}^2 \lambda'_j(P_{\mathrm{m}})}\,\mathbf{S}'(P_{\mathrm{m,ls}})\boldsymbol{X}'_j(P_{\mathrm{m}}), \tag{14}$$

where $r_j \in (0, 1)$ $(j = 1, \ldots, 5)$ are independent uniform random deviates and $\sqrt{\Delta\tilde{\chi}^2}$ is a scaling parameter to be iterated so that the entire orbit solution space is covered and the final results have converged. Initially, one may start with $\Delta\tilde{\chi}^2 = 11.3$ and gradually increase its value. $\mathbf{S}'(P_{\mathrm{m,ls}})$ designates the single s.d. matrix used throughout the interval of the mapping parameter, which allows a straightforward debiasing of the sample orbits at the end of the computation. Here, $\mathbf{S}'(P_{\mathrm{m,ls}})$ is the $\mathbf{S}'$ matrix evaluated at the global least-squares value of the mapping element P_{m}.

In equation (14), we sample the local phase-space volume using the principal-axis directions following from the local linear approximation, after diagonalization by the solution of the eigenproblem in the units specified by the $\mathbf{S}'$ matrix. In the present context, the shape of the local sampling volume is that of a five-dimensional rectangular parallelepiped.

In practical computations, we need to discretize the interval of the mapping element and, after solving the five-dimensional local least-squares problem, interpolate the interval parameters for equation (14).

Once the entire variation interval map is available across the interval of the mapping parameter, trial orbits are generated in the following way. First, a value for the mapping orbital element is obtained from uniform sampling over the mapping interval. Secondly, the remaining five elements are generated by using nearest-neighbour variation intervals of the pre-computed map. Thirdly, the trial orbit qualifies for a sample orbit if it produces an acceptable fit to the observations. Each sample orbit is accompanied by the weight factor

$$w(P_{\mathrm{m}}, \boldsymbol{P}') \propto \sqrt{\det \boldsymbol{\Sigma}^{-1}(P_{\mathrm{m}}, \boldsymbol{P}')}\exp\left[-\frac{1}{2}\chi^2(P_{\mathrm{m}}, \boldsymbol{P}')\right] \times \sqrt{\frac{\lambda'_1(P_{\mathrm{m}}) \cdots \lambda'_5(P_{\mathrm{m}})}{\lambda'_1(P_{\mathrm{m,ls}}) \cdots \lambda'_5(P_{\mathrm{m,ls}})}}. \tag{15}$$

The local linear approximations allow the generation of trial orbits using the five-dimensional Gaussian PDFs. In equation (14), such an alternative approach would entail the replacement of the uniform random deviate factors $(1 - 2r_j)$ by Gaussian deviates, and would result in an additional debiasing Gaussian PDF divisor in equation (15). Such an approach can result in larger numbers of sample orbits close to the line of variation, which can be desirable in cases of heavy computational burden. But, simultaneously, less attention would be paid to the potential solutions further away from the line of variation. In the limit of large numbers of sample orbits, the two approaches yield identical results.

Because of the a priori PDF utilized, the results from VOV sampling are invariant in orbital-element transformations. The choice of the orbital element set is, however, non-trivial as assessed in Section 2.2: the computational speed and applicability of VOV depend on the validity of the local linear approximations as a function of the mapping element.

2.4 Numerical techniques

For exiguous observational data, we make use of Ranging (Muinonen et al. 2001; Virtanen et al. 2001). In Ranging, two observation dates are chosen from the complete observation set. The corresponding topocentric distances (or ranges), as well as the RA and Dec. angles are MC sampled using pre-defined intervals, resulting in altogether 12 interval boundary parameters. The two Cartesian positions lead to an unambiguous set of orbital elements, based on well-established techniques in celestial mechanics (Danby 1992). The following trial orbit qualifies for a sample orbit if and only if it produces an acceptable fit to the entire set of observations. The orbit sampling procedure is repeated to obtain a large number of sample orbits, simultaneously iterating the 12 interval boundary parameters to secure full coverage of the orbit solution space. For extensive observational data, we make use of the least-squares technique (see Muinonen & Bowell 1993, and references therein).

All three methods are implemented in a completely independent software bundle ORB. Our goal is to have a state-of-the-art set of fundamental asteroid orbit computation tools that are easy to use, modify and update. The bundle contains tools such as input and output of different observation formats, input of JPL ephemerides, coordinate and time transformations, several orbital inversion methods, differential correction and integration. Different types of orbital elements can be used during computations, but the Cartesian elements are the

basic ones. Given such a set of tools, more advanced WWW, single-processor or multiprocessor applications for, e.g. the computation of ephemerides, impact monitoring and identification of asteroids, can be put together and maintained. The goal is achieved by using a modern programming language (FORTRAN 95) which allows efficient programs, dynamical memory allocation and parallelization, an object-oriented programming paradigm, advanced documentation tools, and a proper error management, which greatly reduces the time spent on debugging. At present, ORB contains some 20 000 lines of code.

The multitude of numerical integrations of asteroid orbits can become a bottleneck in the software execution time. However, our modular implementation enables us to select the optimum integration technique, or add a new one, without much effort. We currently use both a modified FORTRAN 95 version of the 15th-order RADAU integrator (cf. Everhart 1985) and the Bulirsch–Stoer extrapolation method (Press et al. 1994). The computational load of *N*-body integrations in orbit computation is mostly due to a continuous interpolation of planetary ephemerides. By modifying the RADAU integrator to propagate several massless particles simultaneously, the computational load has been substantially reduced in MC methods. The equations of motion for the asteroid include the Newtonian forces and also the relativistic term due to the Sun (Sitarski 1983).

3 RESULTS AND DISCUSSION

We study the applicability regime for VOV sampling and its implications to the analysis of the phase transition. To study the transition regime, we break down the data for each object night by night and apply the different techniques in a sequential manner to derive the six-dimensional orbital-element PDFs.

The observational data for the NEO 2004 HA_{39}, MBO 2004 QR and the TNO 2002 CX_{224} are available from the Minor Planet Center and correspond to the situation as of 2004 November. 2004 HA_{39} has 57 observations over 145 d from 12 observatories. We considered the following data sets in the order of increasing time interval: 0.027 d (four observations), 0.15 d (eight observations), 0.65 d (26 observations), 0.9 d (30 observations), 2.0 d (34 observations) and 7 d (37 observations). The MBO 2004 QR constitutes a serendipitous discovery during a Nordic observing programme concentrating on NEOs. It was discovered in 2004 August 15 (4 observations), and thereafter followed up on August 17 (observational interval of 2 d; 10 observations), August 22 (7 d; 13 observations) and September 16 (31 d; 16 observations). The full observational interval comprises 19 observations over 39 d. The TNO 2002 CX_{224} has 20 observations over 2 yr from three observatories. The data sets used here are for time intervals of 0.0625 d (two observations), 110 d (five observations), 288 d (eight observations), 411 d (18 observations) and 733 d (20 observations).

Test computations using two-body and *N*-body approaches yielded essentially identical results for the example objects. Thus, two-body approximation is adopted for the present study. The mapping of the semimajor axis was carried out using 1000–50 000 local grid points across the global variation interval, which was typically iterated to be 5–10 times the LSL s.d. values. The scaling factor used for the remaining elements was 1–8. MC computation of a typical sample of 5000 orbits took some 10 min of CPU time on a current workstation. The RA and Dec. rms values of the global least-squares fits for the example objects varied from 0.5 to 1.0 arcsec. Throughout the present work, we assume uncorrelated noise and fix the s.d. of the RA and Dec. errors to 0.5 arcsec for the MBO and the TNO, and to 1.0 arcsec for the NEO.

Fig. 1 shows example one-dimensional marginal PDFs computed using VOV sampling. The a posteriori PDFs are derived both with and without the regularizing a priori PDF. For all the cases, no major differences can be seen in the distributions. This is expected since the orbital-element PDFs are already well-constrained and, in fact, assuming constant a priori would be acceptable in equation (1). There are indications of deviations from bell-shaped Gaussian PDFs for the NEO and TNO.

Fig. 2 shows the extents of the two-dimensional marginal PDFs of the eccentricity, inclination and the mean anomaly against the semimajor axis, with the global least-squares orbital elements given in the captions. For all three objects, the semimajor axis and eccentricity are correlated, supporting the choice of the semimajor axis for the mapping element. Intervals of the coordinate axes are identical to those in Fig. 1. The curvature of the marginal PDFs implies that, for the NEO and TNO, the actual PDFs must be non-Gaussian.

Figs 3–5 show the phase transitions assessed using three computational techniques, i.e. those of Ranging, VOV sampling and LSL. The phase transition takes place at distinctively different times for the different objects: for the NEO, between 0.15 and 0.65 d (3.6 and 15.6 h), for the MBO, between 2 and 7 d, and for the TNO, between 100 and 400 d (3 and 14 months). The results for the NEO and the TNO are consistent with the ones in Virtanen & Muinonen (2006) and Virtanen et al. (2003), respectively.

Note that the results from VOV sampling compare favourably with those from Ranging and LSL for all three objects, whereas LSL sometimes fails for short observational time intervals and Ranging faces difficulties for long intervals.

Fig. 6 shows the time evolution of ephemeris predictions with increasing numbers of observations for the MBA 2004 QR. The collapses (dotted lines) mark the times of the new observations added to the data set. The numbers of the observations are given above and are the same as for the phase-transition study. The uncertainty region becomes well constrained after a week of observations, enabling follow-up observations to be planned several months ahead. Note the decreasing slope in the increasing ephemeris uncertainty after each time new observations are added.

4 CONCLUSIONS

We have described an efficient MC sampling technique for solving the inverse problem of deriving asteroid orbits from transitional observational data, that is, a moderate number of data points spanning a moderate observational time interval. The technique relies on a sequence of local linear approximations that characterize the regime of orbit solutions in the six-dimensional phase space of the orbital elements. Sampling the phase-space volume of variation (VOV sampling), large numbers of sample orbital elements can be generated, describing the rigorous orbital-element probability density function. The potential of VOV sampling has been illustrated via application to NEOs, MBOs and TNOs.

Whereas the current VOV sampling is based on Keplerian elements, is computationally efficient, and agrees with the results from Ranging for short observational time intervals, in the future, we will study the implementation of the technique in Cartesian elements, e.g. using the topocentric range and range rate as the two mapping orbital elements. Currently in VOV sampling, there is two scaling parameters for the mapping orbital element and a third one for the variation intervals of the remaining elements. The technique can be optimized by introducing asymmetric local variation intervals also for the remaining elements.

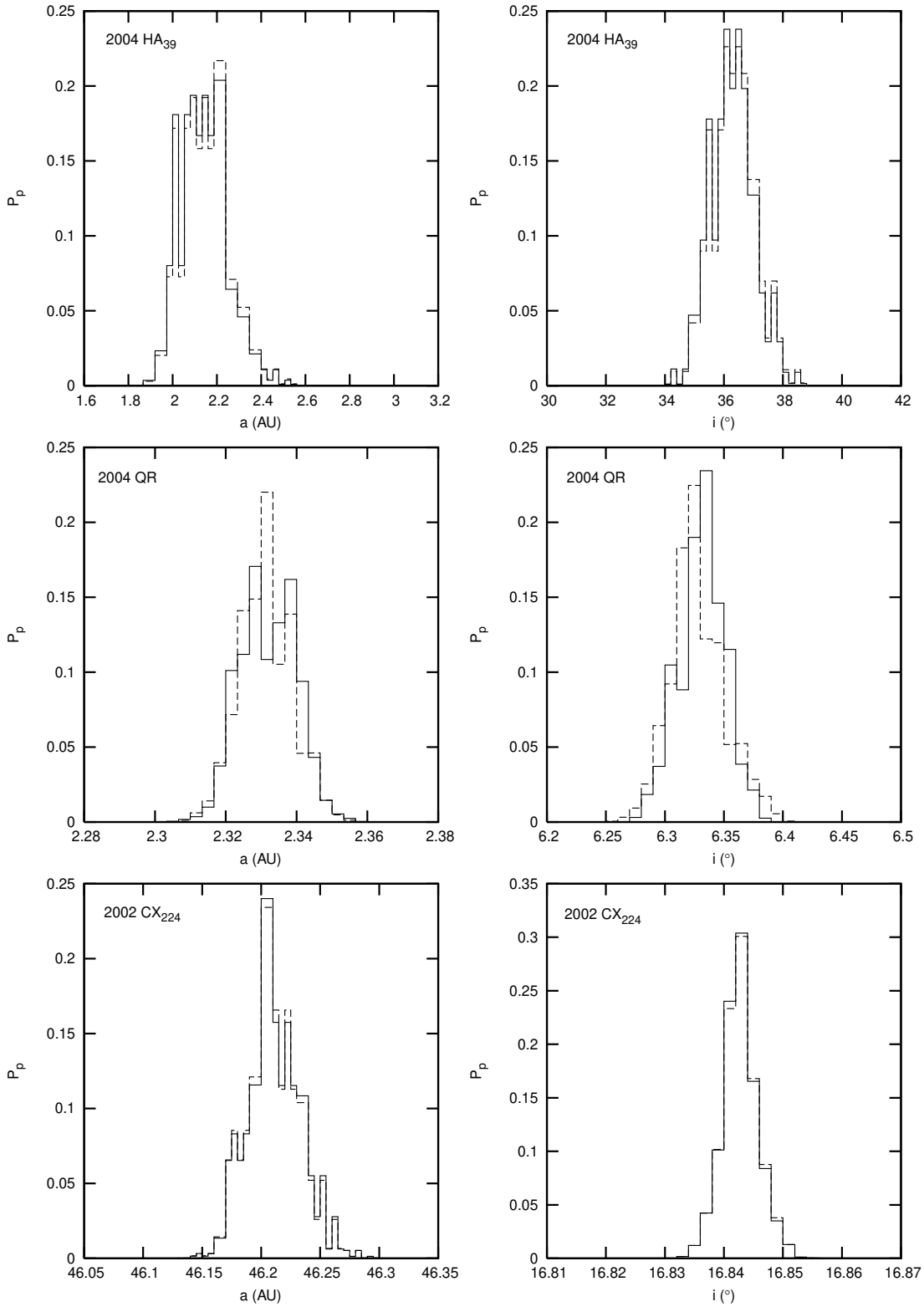

Figure 1. The marginal probability densities for the orbital elements for the NEO 2004 HA_{39} (observational time interval of 0.9 d and an observational error s.d. of 1 arcsec), the MBO 2004 QR (7.2 d and 0.5 arcsec), and the TNO 2002 CX_{224} (733 d and 0.5 arcsec) as computed using VOV sampling (5000 sample orbits). The solid line corresponds to the regularized a posteriori PDF, while the dashed line shows the a posteriori PDF computed without the a priori PDF. For the MBO, the shape of the PDFs is close to a Gaussian one. For the NEO and the TNO, all the marginal PDFs have non-Gaussian features. The bin-size equals $\Delta/30$, where Δ is the interval shown.

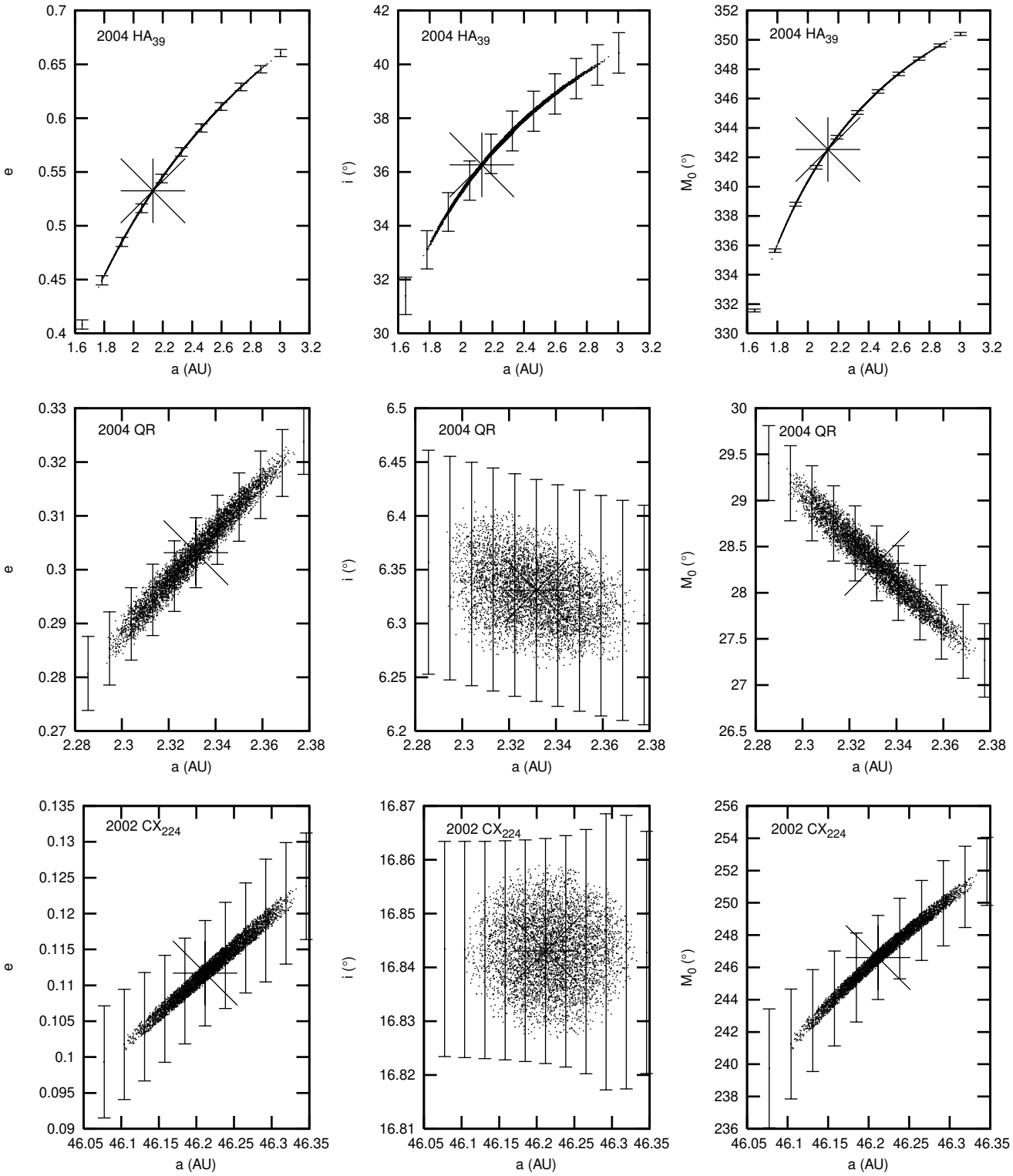

Figure 2. Extents of two-dimensional marginal probability densities for pairs of orbital elements for the NEO 2004 HA_{39} (observational time interval 0.9 d and an observational noise estimate of 1 arcsec), the MBO 2004 QR (7.2 d and 0.5 arcsec), and the TNO 2002 CX_{224} (733 d and 0.5 arcsec) as a function of the mapping parameter, i.e. semimajor axis. LSL solutions (star) are the following 2004 HA_{39} : $a = 2.133$, $e = 0.532$, $i = 36\overset{\circ}{.}268$, $\Omega = 204\overset{\circ}{.}182$, $\omega = 67\overset{\circ}{.}182$, $M_0 = 342\overset{\circ}{.}540$ (epoch 2004 April 25.0 TDT), MBO 2004 QR: $a = 2.332$, $e = 0.303$, $i = 6\overset{\circ}{.}331$, $\Omega = 314\overset{\circ}{.}738$, $\omega = 330\overset{\circ}{.}746$, $M_0 = 28\overset{\circ}{.}320$ (epoch 2004 August 16.0 TDT), 2002 CX_{224} : $a = 46.212$, $e = 0.112$, $i = 16\overset{\circ}{.}843$, $\Omega = 42\overset{\circ}{.}257$, $\omega = 137\overset{\circ}{.}939$, $M_0 = 246\overset{\circ}{.}612$ (epoch 2001 October 21.0 TDT). The iterated variation intervals at selected local linear approximation points for the remaining five elements are shown with the error-bar notation.

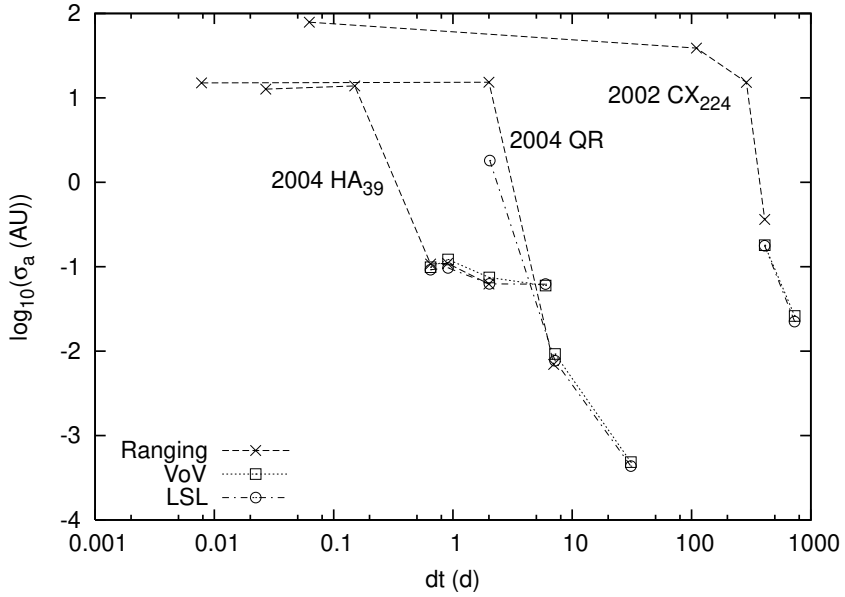

Figure 3. The time evolution of semimajor axis uncertainty for the NEO 2004 HA_{39}, the MBO 2004 QR, and the TNO 2002 CX_{224}. The phase transition takes place between 0.15 and 0.65 d (3.6 and 15.6 h) for 2004 HA_{39}, between 2 and 7 d for 2004 QR and between 100 and 400 d (3 and 14 months) for 2002 CX_{224}.

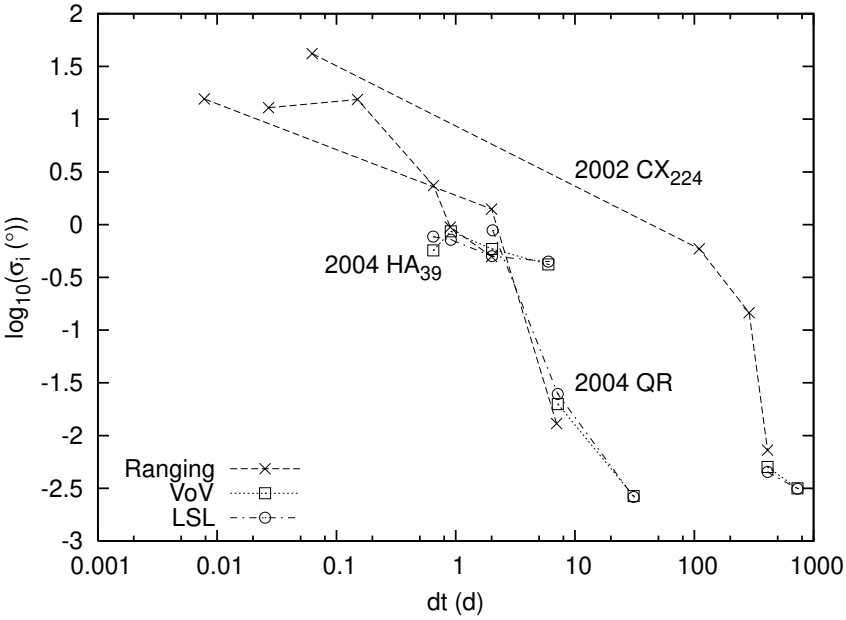

Figure 4. As in Fig. 3, but for eccentricity.

There are prospects for VOV sampling in NEO collision probability computation: in VOV, it is straightforward to constrain the MC sampling into narrow regimes in, e.g. the semimajor axis, allowing densified MC computation of collision probabilities. The densification is often called for as the collision probabilities are typically small, of the order of 10^{-6} or smaller. In continuation, VOV promises to become a useful tool in the assessment of the asteroid identification problem (Granvik et al. 2005).

In comparison to the one-dimensional LOV techniques, such as LOV, the six-dimensional VOV technique has both advantages and disadvantages. Clearly, VOV has the advantage of being able to cover entire six-dimensional volumes of variation which can play a crucial role in, e.g. collision probability computation. By the same token, LOV continues to be the more efficient technique in terms of computing time.

VOV sampling has already proved efficient and useful in the NEO observing programme of the Near-Earth-Object Network at the Nordic Optical Telescope on La Palma (Muinonen et al. 2004). Using the technique, follow-up observational sequences have been designed and successfully realized. The future prospects are intriguing, with application of VOV sampling to the precise astrometry by

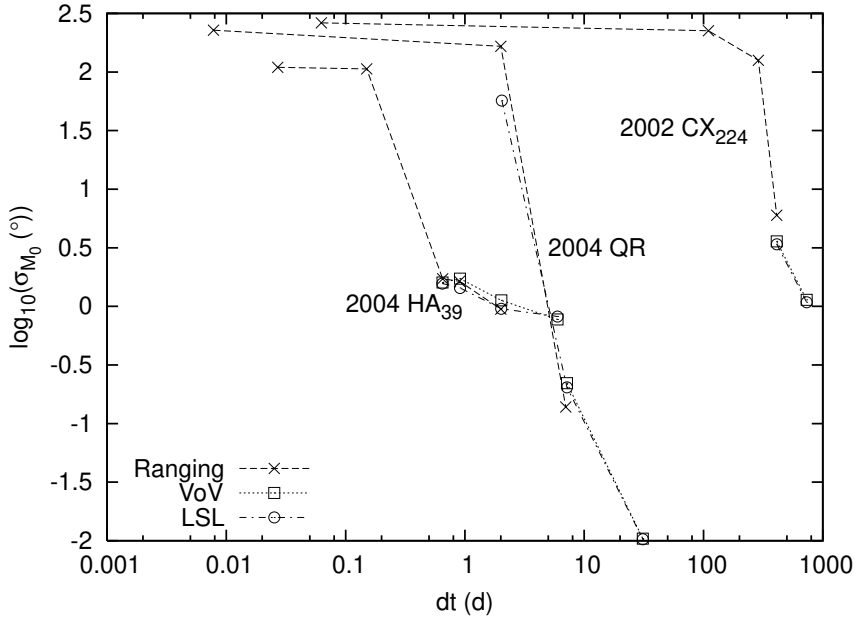

Figure 5. As in Fig. 3, but for inclination.

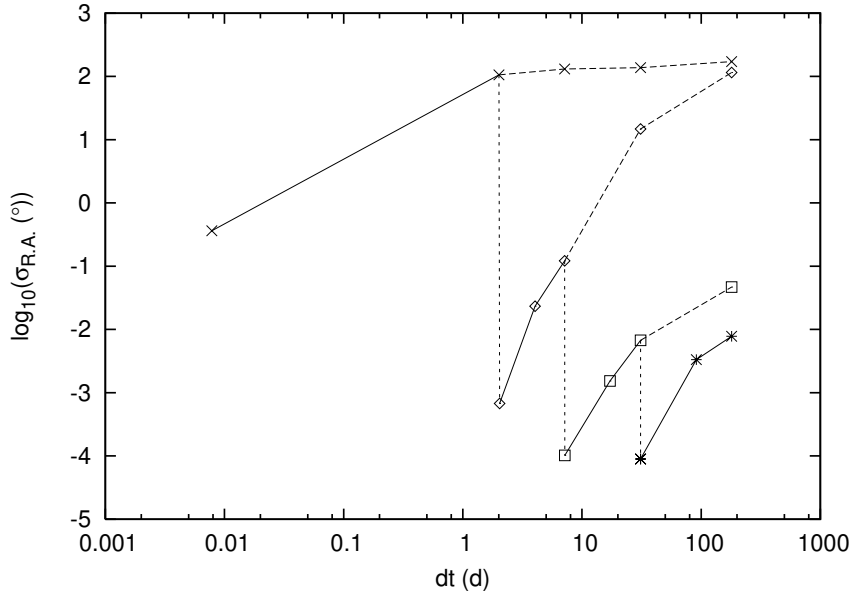

Figure 6. Time evolution of ephemeris uncertainty for 2004 QR. The s.d. of the RA PDFs as a function of time elapsed from discovery for different lengths of the observational time interval, top to bottom: <1 d (crosses; using Ranging), 2.0 d (diamonds; using Ranging), 7.2 d (squares; using Ranging), and 31 d (stars; using VOV). Solid–dashed curves show the evolution of ephemeris prediction; the dashed part corresponds to the hypothetical evolution without the new observations (timing of which is indicated with vertical dotted lines).

Gaia, the ESA astrometric space observatory to be launched no later than 2012.

ACKNOWLEDGMENTS

The research has been supported by the Academy of Finland. Observations for the present work were made, in large part, with the 2.56-m Nordic Optical Telescope, operated on the island of La Palma jointly by Denmark, Finland, Iceland, Norway and Sweden, in the Spanish Observatorio del Roque de los Muchachos of the Instituto de Astrofísica de Canarias.

REFERENCES

Bailey M. E., Emel'yanenko V. V., Hahn G., Harris N. W., Hughes K. A., Muinonen K., Scotti J. V., 1996, MNRAS, 281, 916

Bowell E., Wasserman L. H., Muinonen K., McNaught R. H., West R. M., 1993, BAAS, 25, 1118 (abstract)

Bowell E., Virtanen J., Muinonen K., Boattini A., 2002, in Bottke W., Binzel R. P., Cellino A., Paolicchi P., eds, Asteroids Vol. III. Univ. Arizona Press, Tucson, p. 27

Chesley S. R., 2005, in Knežević Z., Milani A., eds, Proc. IAU Colloq. 197, Dynamics of Populations of Planetary Systems. Cambridge Univ. Press, Cambridge, p. 255

Chesley S. R., Milani A., 1999, in AAS/AIAA Space Flight Mechanics Meeting, Paper 99-148, 16–19 August 1999, Girkwood, Alaska
Danby J. M. A., 1992, Fundamentals of Celestial Mechanics. Willmann-Bell, Inc., Richmond, VA
Everhart E., 1985, in Carusi, A., Valsecchi G. B., eds, Dynamics of Comets: Their Origin and Evolution. Reidel, Dordrecht, p. 185
Gauss C. F., 1809, Theory of the Motion of the Heavenly Bodies Moving About the Sun in Conic Sections. Dover, New York, p. 326 (1963)
Granvik M. et al., 2005, in Knežević Z., Milani A., eds, Proc. IAU Colloq. 197, Dynamics of Populations of Planetary Systems. Cambridge Univ. Press, Cambridge, p. 231
Jeffreys H., 1946, Proc. R. Stat. Soc. London, Ser. A, 186, 453
Milani A., 1999, Icarus, 137, 269
Milani A., Chesley S. R., Chodas P. W., Valsecchi G. B., 2002, in Bottke W., Binzel R. P., Cellino A., Paolicchi P., eds, Asteroids III. Univ. Arizona Press, Tucson, p. 55
Milani A., Gronchi G. F., Vitturi M. D., Knežević Z., 2004, Celest. Mech. Dyn. Astron., 90, 57
Milani A., Gronchi G. F., Knežević Z., Sansaturio M. E., Arratia O., 2005, Icarus, 179, 350
Muinonen K., 1996, MNRAS, 280, 1235
Muinonen K., Bowell E., 1993, Icarus, 104, 255
Muinonen K., Virtanen J., 2002, in Isobe S., Asakura Y., eds, International Workshop on Collaboration and Coordination Among NEO Observers and Orbit Computers. Japan Spaceguard Association, p. 105
Muinonen K., Milani A., Bowell E., 1997, in Wytrzyszczak I. M., Lieske J. H., Feldman R. A., eds, Proc. IAU Colloq. 165, Dynamics and Astrometry of Natural and Artificial Celestial Bodies. Kluwer, Dordrecht, p. 191
Muinonen K., Virtanen J., Bowell E., 2001, Celest. Mech. Dyn. Astron., 81, 93
Muinonen K. et al., 2004, BAAS, 36, 1185 (abstract)
Press W. H., Flannery B. P., Teukolsky S. A., Vetterling W. T., 1994, Numerical Recipes, The Art of Scientific Computing, 2nd edn. Cambridge Univ. Press, Cambridge
Reichl L. E., 1980, A Modern Course in Statistical Physics. Univ. Texas Press, Austin
Sitarski G., 1983, Acta Astron., 33, 295
Virtanen J., Muinonen K., 2006, Icarus, submitted
Virtanen J., Muinonen K., Bowell E., 2001, Icarus, 154, 412
Virtanen J., Tancredi G., Muinonen K., Bowell E., 2003, Icarus, 161, 419
Virtanen J., Muinonen K., Granvik M., Laakso T., 2005, in Knežević Z., Milani A., eds, Proc. IAU Colloq. 197, Dynamics of Populations of Planetary Systems. Cambridge Univ. Press, Cambridge, p. 239

This paper has been typeset from a TEX/LATEX file prepared by the author.